Development of a Novel Active Polypyrrole Trilayer Membrane

Jingwen Wang,[†] Steven J. Botelho,[†] Hani E. Naguib,[†,‡] and Aimy Bazylak*[,†,§]

[†]Department of Mechanical & Industrial Engineering [‡]Smart & Adaptive Polymers Lab [§]Microscale Energy Systems Transport Phenomena Laboratory, Faculty of Applied Science and Engineering, University of Toronto, 5 King's College Road Toronto, Ontario, Canada, M5S 3G8

ABSTRACT: In this work, a novel design of an active trilayer polymer membrane formed by doped polypyrrole (PPy) is presented. The PPy trilayer membrane was synthesized with a bis(trifluoro-methane)-sulfonimide lithium salt (LiTFSI) dopant and was electrochemically deposited onto a gold-coated polyvinylidene fluoride porous membrane within a custom-designed electrochemical cell. The effects of the polymerization current density and activation potential on surface properties such as roughness, wrinkling, and wettability of the PPy trilayer membrane, were determined. The surface properties of membranes fabricated at five polymerization current densities, i_p, were compared. These membranes were activated at potentials ranging between 0 and 2 V. The membrane fabricated with i_p = 0.1 mA/cm^2 exhibited the most dynamic range of surface properties as a function of activation potential, with a maximum increase in wrinkled area of 37%, surface roughness of 200%, and apparent contact angle from 55° to 96°. The actively tunable surface properties of this novel membrane provide promising opportunities for the development of surface reaction-based clean energy technologies.

KEYWORDS: Active, Electroactive polymer, Polypyrrole, Trilayer membrane, Wettability

INTRODUCTION

Electroactive polymers (EAPs) have been widely applied over the past two decades. Because of their high electronic and ionic conductivities, fast charge and discharge rates, and ability to provide large active reaction sites,[1] EAPs have been studied in various energy applications, including dye-sensitized solar cell counter electrodes,[2–5] modified Nafion membranes in fuel cells,[6–10] platinum catalyst supports,[11,12] corrosion-resistive coatings for fuel cell bipolar plates,[13,14] and novel electrode materials for supercapacitors and batteries.[15–19] EAPs are also attractive for the advantages they provide through their redox switching properties,[1] which enable electrical stimulation of mechanical, electrical, and surface property changes.

Polypyrrole (PPy) is an EAP with mobile ions that can be driven by an external electric field to induce swelling or contraction. PPy is of particular interest because of its ease of synthesis, high electrical conductivity, environmental stability,[1] and biocompatibility.[20] PPy is a conjugated polymer with alternating single and double carbon bonds in the polymer backbone. PPy can be easily oxidized and reduced. When an oxidative potential is applied, electrons in the polymer chain are removed, resulting in an increase in the number of positive charge carriers.[21] When the PPy layer is in contact with an electrolyte, mobile ions in the electrolyte and the dopant are exchanged to maintain charge neutrality. The buildup or loss of ions from the PPy layer causes it to expand or contract.[21] When the mobile ions are cationic, the PPy layer will expand during reduction and contract during oxidation. The opposite effect occurs for a system with mobile anions. These properties have

made PPy attractive for a number of applications, including sensors,[22] actuators,[23] electro-chromic devices,[24] artificial muscles,[25] and biomimetic robotics.[26]

Active PPy membranes have been studied primarily for their actuation behavior, such as their high strain capabilities and fast redox responses.[21,26–28] In Fang et al.,[21] the authors fabricated and measured the joint force-displacement of a trilayer PPy actuator to validate their proposed scalable model for actuation behavior. Research has also focused on volume changes of single layer PPy films[29,30] and surface property changes of such single layer films during activation.[31–33] Chainet et al. measured the surface roughness of lithium perchlorate-doped polypyrrole (PPy(ClO$_4$)) film on a platinum electrode using scanning tunnelling microscopy.[32] Upon application of activation potentials between −0.5 and 0.1 V, the mean surface roughness decreased from 219 to 75 nm. The authors attributed this decrease in surface roughness to uneven membrane swelling. Teh et al. measured the change in the apparent contact angle of sodium dodecylbenzenesulfonate-doped polypyrrole (PPy-(DBS)) films due to applied activation potentials ranging from −0.9 to 0.9 V, and they found that the contact angle increased by 60°.[33]

Previous work has illustrated the range of surface property changes that are possible with PPy films; however, in the studies discussed above, PPy films required immersion in an

aqueous electrolyte for activation. To provide functionality in dry environments, we have developed a novel active PPy trilayer membrane that can function without electrolyte immersion. For the PPy trilayer membrane discussed in this paper, the electrolyte is contained within the porous core layer, isolated between PPy layers from the ambient environment. In this work, we discuss the development of this novel designed PPy trilayer membrane and investigate the range of surface properties that are exhibited as a function of activation potential. These surface properties include surface roughness, wrinkling, and wettability (contact angle). To the best of our knowledge, this is the first investigation of these tunable surface properties for a PPy trilayer membrane.

■ EXPERIMENTAL MATERIALS

Pyrrole (Py) monomer (MW: 67.09), bis(trifluoromethane)-sulfonimide lithium salt (LiTFSI) (MW: 287.09), propylene carbonate (PC) (99.7%), and polyvinylidine difluoride (PVDF) membranes were purchased from Sigma Aldrich. The Pyrrole monomer was purified and stored at 4 °C in darkness prior to use. It is important to note that the PVDF membrane serves as the core of the PPy trilayer membrane.

Fabrication with Electrochemical Deposition. To fabricate the trilayer membrane, a custom-built electrochemical cell shown in Figure 1 was employed. PVDF membranes were sputter-coated with gold
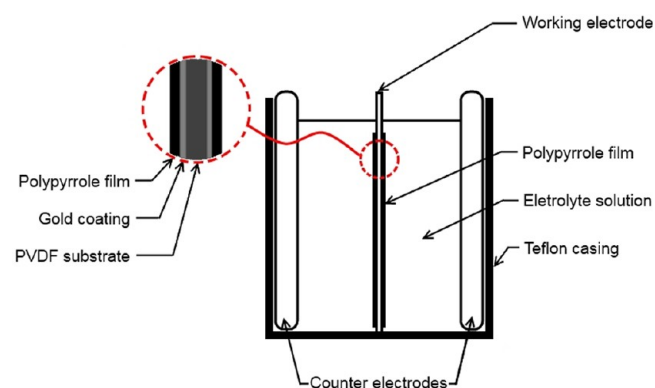

Figure 1. Schematic of the electrochemical cell apparatus employed for the electro-polymerization of PPy.

(99.99% purity, ~21 nm thick) on both sides using a sputter coater (EMS 7620, Electron Microscopy Sciences US) to create conductive surfaces that served as the working electrodes for polymer deposition. Two stainless steel plates placed on either side of the chamber were used as counter electrodes. An electrolytic solution was prepared by combining 0.3 M Py monomer, 0.2 M of LiTFSI, and 1% w/w deionized water in PC. This mixture was stirred for 15 min until homogeneity was achieved and then poured into the electrochemical cell chamber for polymerization.

Current was applied to the working electrode with a Keithley 2400 Sourcemeter (Keithley Instrument, Inc., Cleveland OH), where five current densities between 0.05 and 1.00 mA/cm² were applied (Table 1) to fabricate membranes with distinct surface morphologies. In order to optimize the ionic conductivity of the specimen, the electro-polymerization process was conducted at −30 °C.[11] This process was done for 6 h to form the PPy(TFSI) trilayer membranes with dimensions of 50 mm × 50 mm. This resulted in a PPy(TFSI) trilayer membrane that consisted of a PVDF core layer saturated with electrolyte (containing TFSI⁻ mobile ions). The trilayer membranes were cut into sample sizes of 5 mm × 25 mm and stored in an electrolyte solution containing 0.2 M LiTFSI in PC prior to use.

Methodology for Morphological Characterization. To obtain high spatial resolution images of the membranes prior to activation, the fabricated PPy(TFSI) samples were dried under vacuum (−30

Table 1. Summary of Fabrication Conditions for the Membranes Investigated[a]

Membrane	i_p (mA/cm²)
A	0.05
B	0.10
C	0.30
D	0.50
E	1.00

[a]All membranes were polymerized for 6 h.

inHg) at room temperature for ~12 h before being imaged with a scanning electron microscope (SEM) (JEOL-JSM-6060 Akishima Tokyo, Japan). Nodule formations were analyzed with ImageJ software. Once samples were imaged using the SEM, they were no longer employed for further activation-based investigations. New samples were employed for the activation-based investigations described below.

Before each activation experiment, the PPy(TFSI) trilayer membrane was removed from the electrolyte, and the surface was blotted dry with a Kimwipe prior to activation to remove excess electrolyte. The bottom surface of the membrane was then adhered to a glass slide with double-sided tape (3M Canada, London, Canada). The tape was employed to restrict the bending motion of the membrane in order to isolate the changes in surface properties. Electrodes were placed on both sides of the trilayer membrane as shown in Figure 2(b), and four activation potentials (V_a = 0.5, 1.0, 1.5,
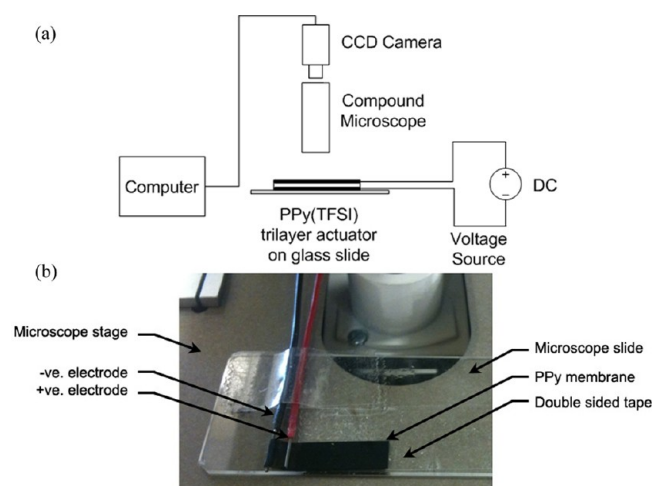

Figure 2. (a) Schematic showing the microscopy-based apparatus employed for measuring surface wrinkles during material activation. Raw images were collected by the CCD camera and uploaded to the computer. (b) Image showing the placement of the electrodes on PPy membrane that is fixed onto a glass slide.

and 2.0 V) were applied to the membrane in succession for approximately 1 min at each potential. Positive potentials were applied to induce membrane expansion during oxidation (mobile anions were TFSI⁻ ions). These activation potentials were also chosen to be in the range that is typically employed for ionic EAPs.[34] After each sample was activated for 1 min, it was again blotted dry due to the emergence of electrolyte at the surface.

The electrodes were removed from the membrane before the visualization was performed for each of the studies described in detail below. It is important to note that the visualizations were captured within a 10 min time frame after ceasing activation, during which the materials maintained their activated surface properties. After the 10 min time frame, the materials slowly relaxed to their unactivated states. This was verified through an optical image-based sensitivity study where the measured surface properties as a function of time were

compared. Raw images captured during activation and 10 min after activation were ceased and only varied by 0.5% in a pixel-by-pixel based intensity comparison.

Surface Wrinkle Measurements. For surface wrinkle analysis that demonstrates the in-plane activation effects on surface morphology, the PPy membrane was imaged from above with a high-resolution CCD camera (PCO Pixelfly, Kelheim, Germany) combined with a compound microscope (Leica DM2500 M, Wetzler, Germany) as shown in Figure 2(a). Visualizations with a 20× objective were performed prior to and after each activation. The surface wrinkle formation was analyzed using a custom image processing procedure in Matlab. To analyze this wrinkling effect, the raw images were first converted to binary images with a threshold value of 0.31 (chosen to maximize the detection of wrinkles). Every pixel with brightness below the threshold was set to 0 (black). Objects with circularity less than 0.2 were considered as wrinkles. Circularity is defined as the following

$$Circularity = 4\pi(A/P^2)$$

where A and P represent area and perimeter of the object of interest respectively. Based on this definition, the circularity for a circle is 1. The percentage increase of wrinkled area ($\Delta\varepsilon$) on each image was calculated with the following:

$$\Delta\varepsilon = \varepsilon_{@Va} - \varepsilon_o$$

where $\varepsilon_{@Va}$ and ε_o represent wrinkled area at each activation potential and wrinkled area at $V_a = 0$ V respectively.

Surface Roughness Measurements. In addition to in-plane effects, through-plane activation effects on surface morphology were evaluated through surface roughness (Ra) measurements with a Surface Roughness Tester (Times, Inc. TR200). From a sensitivity analysis, a measurement length of 50 mm was chosen to best represent the roughness of the membrane surface. Following the activation at each potential, the membrane was placed under the surface roughness tester. A new sample was employed for each measurement. The averaged Ra values from three sets of measurements were collected at each V_a.

To examine surface wettability changes during activation due to the in-plane and through-plane effects, apparent contact angles (θ) for liquid water droplets on the membrane surfaces were also measured at each V_a. The side views of the droplets were imaged with a macroscope (Leica Z16 APO, Wetzler, Germany). The macroscope is employed for its capability for imaging at long depth of fields. Liquid water was dyed with a dilute solution of fluorescein to enhance the detection of the liquid/gas and liquid/solid interfaces. Water droplets (~3 μL) were dispensed with a micropipet (Finnpipette, Thermo Fisher Scientific, Inc., Waltham, MA) onto the membrane surface. At each activation potential, an average apparent contact angle was determined from measurements of 10 separate droplets within a region of 5 mm × 5 mm. The images were captured with a high resolution CCD camera (PCO 1600, Kelheim, Germany) and processed with software developed in-house using Matlab.

■ RESULTS AND DISCUSSION

We investigated the surface property tunability of PPy trilayer membranes fabricated at various current densities. These surface properties included: surface wrinkling, surface roughness, and wettability over a range of applied potentials. Even in the absence of electrical activation, we found that the current density applied during membrane fabrication made a significant impact on the surface morphology of the material. In particular, membranes B and E, fabricated with $i_p = 0.1$ mA/cm^2 and $i_p = 1.0$ mA/cm^2, respectively, exhibited the most drastic differences in nodule formation and distribution. SEM images of membranes B and E are shown in Figure 3. The surface of membrane B shown in Figure 3(a) ($i_p = 0.1$ mA/cm^2) was generally uniform, exhibiting small and uniformly spaced nodules with diameters ranging from 1 to 3 μm. In contrast,
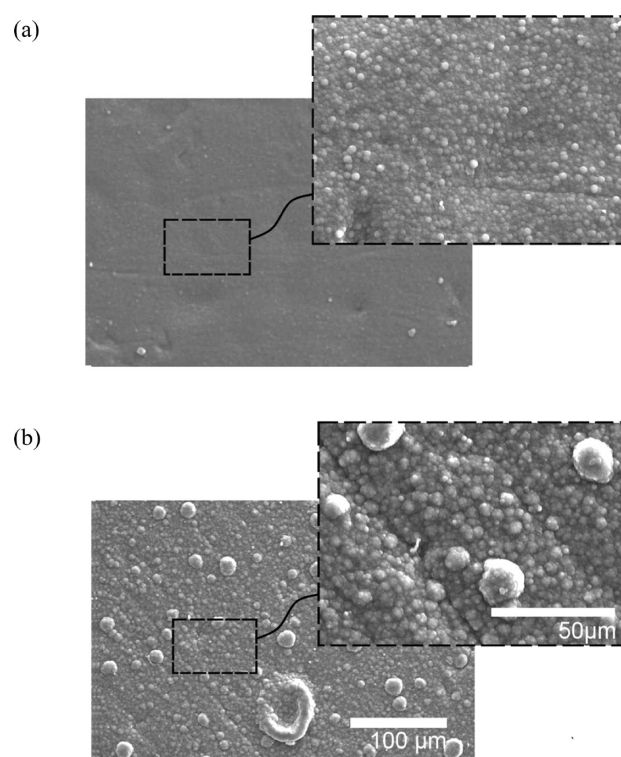

(a)

(b)

Figure 3. SEM images of PPy trilayer membranes fabricated with $i_p = 0.1$ mA/cm^2 (membrane B) and $i_p = 1.0$ mA/cm^2 (membrane E). (a) Membrane B at 200× and 500× magnification. (b) Membrane E at 200× and 500× magnification.

membrane E shown in Figure 3(b) ($i_p = 1.0$ mA/cm^2) exhibited larger, cauliflower-shaped nodules with diameters ranging from 2 to 8 μm. Nonhomogeneously distributed larger nodules with diameters from 10 to 20 μm were also observed on membrane E.

Effect of Activation Potential on Planar Wrinkling. Figure 4 shows optical images taken when membrane B was activated from 0 to 2 V, in increments of 0.5 V. As shown in this figure, the degree of wrinkling increased with increasing activation potential. Similar behavior was observed for all other membranes. When a positive potential was applied to the trilayer membrane, the PPy layer in contact with the positive electrode became more positively charged. In order to maintain charge neutrality, mobile TFSI$^-$ ions from the electrolyte were incorporated into the polymer chain, resulting in polymer chain expansion. If the membrane was free to move, the swelling of the membrane would result in trilayer membrane bending. Because the bottom surface of the membrane was fixed, we were able to isolate activation effects as morphological changes, where the expansion of polymer chains was translated into wrinkle formation.

Figure 5 illustrates the percentage increase in wrinkled area as a function of V_a for all five membranes. Six trials were analyzed for each membrane. Similar trends were observed in all six trials, and a representative trial for each membrane is presented in Figure 5. For all membranes, as V_a increased, the percentage increase of wrinkled area, $\Delta\varepsilon$, increased. From $V_a = 0$ to 2 V, membrane B exhibited the largest increase in wrinkled area (37% increase), and membrane C had the next largest increase in wrinkled area (25% increase). Membranes A, D, and E exhibited significantly smaller changes (less than 10%).
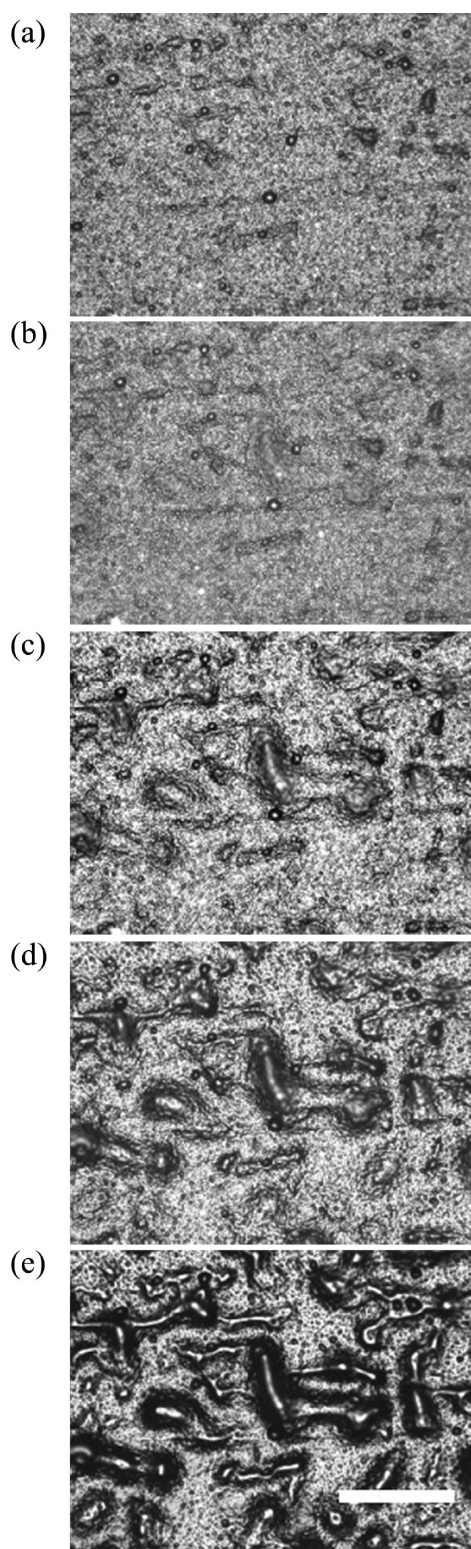
Figure 4. Optical images of a trilayer PPy membrane fabricated with an i_p of 0.1 mA/cm², showing the changes in surface morphology associated with V_a = (a) 0 V, (b) 0.5 V, (c) 1.0 V, (d) 1.5 V, and (e) 2.0 V. Each activation took place for 1 min before photo was taken. The length bar represents 150 μm.

From Figure 5, we see that increasing the applied current density during membrane fabrication, i_p, beyond 0.3 mA/cm² does not result in increased wrinkle tunability (membranes D and E). This is attributed to the increase in membrane
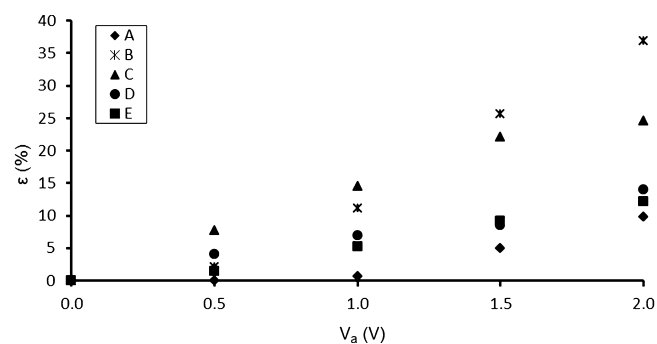

Figure 5. Percentage of wrinkled area increase as a function of V_a, where the most significant increase in wrinkled area was observed for membrane B.

thickness that is associated with increasing i_p. When the membrane thickness increases, the membrane becomes more rigid and more potential mobile ions become immobilized. This results in creating fewer available chains for TFSI⁻ ion attachment, thereby reducing the effect of activation on surface wrinkling. This phenomenon is in agreement with the work of Dziewonski et al.,[35] where the authors explained that the film thickness is proportional to fabrication current density, and as the film thickness increases, more anions are immobilized.

A small degree of wrinkling was also observed for i_p values less than 0.1 mA/cm² during fabrication. This is attributed to the decreased availability of polymer chains for ionic diffusion during activation for thin membranes.

Effect of Activation Potential on Surface Roughness.
Figure 6 illustrates the surface roughness values, Ra, measured using the surface roughness tester. The averaged Ra values from three sets of measurements at each activation potential are shown, where two regions of interest are identified. For membranes B and C, the overall increase in Ra from 0 to 2 V was approximately 200%. For membranes A, D, and E, the increases in Ra values were approximately 60−90%. As shown in Figure 6, larger standard deviations were associated with high V_a, especially for membranes fabricated with higher i_p. This may be attributed to the nonuniform nodule formation associated with higher i_p. Prior to activation, the surface roughness increased with increasing current density, which is consistent with the nodule sizes visualized in the SEM images (Figure 3). The amount of change in Ra values also corresponded to planar wrinkle formations for the membranes, where membrane B (i_p = 0.1 mA/cm²) showed the highest degree of surface morphology changes in roughness values as well as the most significant change in wrinkle formation. It is noteworthy that these changes were much greater in the through-plane direction (roughness) compared to the in-plane direction (wrinkles).

Effects of Activation Potential on Apparent Contact angle. Figure 7 shows that the apparent contact angle is a function of increasing activation potential for 3 μL droplets, where the maximum standard deviation for the 10 measurements was 3°. At 0 V, $θ$ is increasing with i_p, which is also in agreement with the Ra measurements, i.e., increasing i_p resulted in increased surface roughness. An approximately linearly increasing trend is observed for the membrane apparent contact angle during activation. Membrane B has the largest increase in apparent contact angle during activation, from 55° to 96°. The wetting properties of membranes B and E changed from hydrophilic to hydrophobic after a 2 V activation. This increase in apparent contact angle is attributed to the observed increase
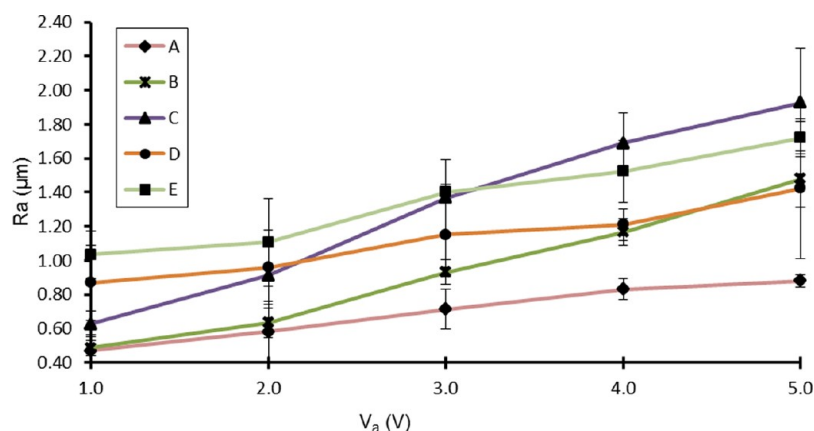
Figure 6. Impact of activation potentials on surface roughness. Membranes A, D, and E provide an overall increase (∼70%) in surface roughness, Ra, with increasing activation potential, V_a. In contrast, membranes B and C provide significant increases (∼200%) in Ra with increasing V_a.
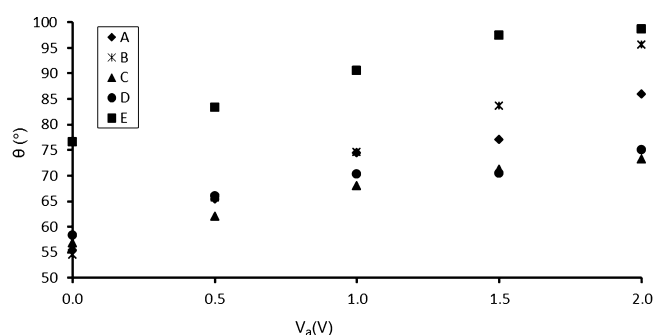

Figure 7. Relationship between the apparent contact angle, θ, and V_a. An increase in θ was observed for all 5 membranes, where membrane B had the most overall increase in θ measurements. The maximum standard deviation for each θ is 3°.

in surface roughness.[36] It is interesting to note that the effects of activation at the molecular level extend to macro-scale effects on the material observed through changes in wrinkle formation, surface roughness, and apparent contact angle measurements.

CONCLUSION

In this work, a novel design of an active membrane using a PPy trilayer membrane was developed, and a strong relationship was identified between polymerization current density and activation potential on membrane tunability of surface wrinkling, wettability, and roughness. Five conductive PPy trilayer membranes were electropolymerized from an electrolyte solution containing Py monomers onto a porous PVDF core at current densities ranging from 0.05 to 1.00 mA/cm². The trilayer membranes were activated at applied activation potentials ranging from 0 to 2 V. It was shown that the applied current density during fabrication affected the structural formation of the PPy membranes, which in turn influenced the surface property tunability of the membranes. It was shown that the wrinkled area, surface roughness, and apparent contact angles increased as the activation potential increased for all membranes. In particular, membrane B (i_p = 0.1 mA/cm²) exhibited the greatest change in all three parameters with maximum increase of 37% in wrinkled area, 200% in surface roughness, and 41° in apparent contact angle. Thicker membranes were fabricated at current densities above 0.30 mA/cm², resulting in membranes with higher stiffness, increased numbers of immobilized ions, and an overall

reduction in available reaction sites. Thinner membranes fabricated at current densities below 0.1 mA/cm² were also unfavorable for surface property tunability due to their insufficient number of reaction sites. For the range of fabrication current densities investigated in this study, membrane B was the most desirable for exhibiting highly tunable surface properties through electrical activation. The results showcased in this study can be implemented into clean energy technologies that are dependent on surface morphology.

AUTHOR INFORMATION

Corresponding Author

*E-mail: abazylak@mie.utoronto.ca. Phone: 1-416-946-5031. Fax: 1-416-978-7753.

Notes

The authors declare no competing financial interest.

REFERENCES

(1) Wallace, G. G. *Conductive Electroactive Polymers: Intelligent Materials System*; CRC Press LLC: Boca Raton, FL, 2003.
(2) Zhang, J.; Hreid, T.; Li, X.; Guo, W.; Wang, L.; Shi, X.; Su, H.; Yuan, Z. Nanostructured polyaniline counter electrode for dye-sensitised solar cells: Fabrication and investigation of its electrochemical formation mechanism. *Electrochim. Acta* **2010**, *55*, 3664–3668.
(3) Mohan Kumar, G.; Raman, V.; Kawakita, J.; Ilanchezhiyan, P.; Jayavel, R. Fabrication of polypyrrole/ZnCoO nanohybrid systems for solar cell applications. *Dalton Trans.* **2010**, *39*, 8325–8330.
(4) Makris, T.; Dracopoulos, V.; Stergiopoulos, T.; Lianos, P. A quasi solid-state dye-sensitized solar cell made of polypyrrole counter electrodes. *Electrochim. Acta* **2011**, *56*, 2004–2008.
(5) Xiaoming, F.; Xianwei, H.; Zhuo, T.; Bin, Z.; Songting, T. Application research of polypyrrole/graphite composite counter electrode for dye-sensitized solar cells. *Acta Chim. Sin.* **2011**, *69*, 653–658.
(6) Cindrella, L.; Kannan, A. M. Membrane electrode assembly with doped polyaniline interlayer for proton exchange membrane fuel cells

230

dx.doi.org/10.1021/sc300078v | *ACS Sustainable Chem. Eng.* 2013, 1, 226–231

under low relative humidity conditions. *J. Power Sources.* **2009**, *193*, 447−453.

(7) Huang, Q. M.; Zhang, Q. L.; Huang, H. L.; Li, W. S.; Huang, Y. J.; Luo, J. L. Methanol permeability and proton conductivity of Nafion membranes modified electrochemically with polyaniline. *J. Power Sources.* **2008**, *184*, 338−343.

(8) Smit, M. A.; Ocampo, A. L.; Espinosa-Medina, M. A.; Sebastian, P. J. A modified Nafion membrane with in situ polymerized polypyrrole for the direct methanol fuel cell. *J. Power Sources* **2003**, *124*, 59−64.

(9) Xia, J.; Chen, L.; Yanagida, S. Application of polypyrrole as a counter electrode for a dye-sensitized solar cell. *J. Mater. Chem.* **2011**, *21*, 4644−4649.

(10) Yang, J.; Shen, P. K.; Varcoe, J.; Wei, Z. Nafion/polyaniline composite membranes specifically designed to allow proton exchange membrane fuel cells operation at low humidity. *J. Power Sources* **2009**, *189*, 1016−1019.

(11) Huang, S.; Ganesan, P.; Popov, B. N. Development of conducting polypyrrole as corrosion-resistant catalyst support for polymer electrolyte membrane fuel cell (PEMFC) application. *Appl. Catal., B* **2009**, *93*, 75−81.

(12) Unni, S. M.; Dhavale, V. M.; Pillai, V. K.; Kurungot, S. High Pt utilization electrodes for polymer electrolyte membrane fuel cells by dispersing Pt particles formed by a preprecipitation method on carbon "polished" with polypyrrole. *J. Phys. Chem. C* **2010**, *114*, 14654−14661.

(13) Antunes, R. A.; Oliveira, M. C. L.; Ett, G.; Ett, V. Corrosion of metal bipolar plates for PEM fuel cells: A review. *Int. J. Hydrogen Energy* **2010**, *35*, 3632−3647.

(14) Joseph, S.; McClure, J. C.; Sebastian, P. J.; Moreira, J.; Valenzuela, E. Polyaniline and polypyrrole coatings on aluminum for PEM fuel cell bipolar plates. *J. Power Sources* **2008**, *177*, 161−166.

(15) Cui, L.; Shen, J.; Cheng, F.; Tao, Z.; Chen, J. SnO_2 nanoparticles-polypyrrole nanowires composite as anode materials for rechargeable lithium-ion batteries. *J. Power Sources* **2011**, *196*, 2195−2201.

(16) Paul, S.; Lee, Y.; Choi, J.; Kang, Y. C.; Kim, D. Synthesis and electrochemical characterization of polypyrrole/multi-walled carbon nanotube composite electrodes for supercapacitor applications. *Bull. Korean Chem. Soc.* **2010**, *31*, 1228−1232.

(17) Snook, G. A.; Kao, P.; Best, A. S. Conducting-polymer-based supercapacitor devices and electrodes. *J. Power Sources* **2011**, *196*, 1−12.

(18) Sun, W.; Zheng, R.; Chen, X. Symmetric redox supercapacitor based on micro-fabrication with three-dimensional polypyrrole electrodes. *J. Power Sources* **2010**, *195*, 7120−7125.

(19) Guo, Z.; Wang, J.; Liu, H.; Dou, S. Study of silicon/polypyrrole composite as anode materials for Li-ion batteries. *J. Power Sources* **2005**, *146*, 448−451.

(20) Mao, C.; Zhu, A.; Wu, Q.; Chen, X.; Kim, J.; Shen, J. New biocompatible polypyrrole-based films with good blood compatibility and high electrical conductivity. *Colloids Surf., B* **2008**, *67*, 41−45.

(21) Fang, Y.; Tan, X.; Shen, Y.; Xi, N.; Alici, G. A scalable model for trilayer conjugated polymer actuators and its experimental validation. *Mater. Sci. Eng., C* **2008**, *28*, 421−428.

(22) Waghuley, S. A.; Yenorkar, S. M.; Yawale, S. S.; Yawale, S. P. Application of chemically synthesized conducting polymer-polypyrrole as a carbon dioxide gas sensor. *Sens. Actuators, B* **2008**, *128*, 366−373.

(23) Hutchison, A. S.; Lewis, T. W.; Moulton, S. E.; Spinks, G. M.; Wallace, G. G. Development of polypyrrole-based electromechanical actuators. *Synth. Met.* **2000**, *113*, 121−127.

(24) Shibata, M.; Kawashita, K.; Yosomiya, R.; Gongzheng, Z. Electrochromic properties of polypyrrole composite films in solid polymer electrolyte. *Eur. Polym. J.* **2001**, *37*, 915−919.

(25) Mirfakhrai, T.; Madden, J. D. W.; Baughman, R. H. Polymer artificial muscles. *Mater. Today* **2007**, *10*, 30−38.

(26) Price, A.D.; Naguib, H.E.; , Characterization of conductive polymer trilayer actuators for biomimetic robotics, (2008) 325-334.

(27) Wu, Y.; Alici, G.; Spinks, G. M.; Wallace, G. G. Fast trilayer polypyrrole bending actuators for high speed applications. *Synth. Met.* **2006**, *156*, 1017−1022.

(28) Chan, C.; Chang, S.; Naguib, H. E. Development and characterization of polypyrrole bi-layer and tri-layer thin porous films. *Smart Mater. Struct.* **2009**, *18*, 104022.

(29) Suárez, M. F.; Compton, R. G. In situ atomic force microscopy study of polypyrrole synthesis and the volume changes induced by oxidation and reduction of the polymer. *J. Electroanal. Chem.* **1999**, *462*, 211−221.

(30) Smela, E.; Gadegaard, N. Volume change in polypyrrole studied by atomic force microscopy. *J. Phys. Chem. B* **2001**, *105*, 9395−9405.

(31) Li, J.; Wang, E.; Green, M.; West, P. E. In situ AFM study of the surface morphology of polypyrrole film. *Synth. Met.* **1995**, *74*, 127−131.

(32) Chainet, E.; Billon, M. In situ study of polypyrrole morphology by STM: effect of the doping state. *J. Electroanal. Chem.* **1998**, *451*, 273−277.

(33) Teh, K. S.; Takahashi, Y.; Yao, Z.; Lu, Y. Influence of redox-induced restructuring of polypyrrole on its surface morphology and wettability. *Sens. Actuators, A* **2009**, *155*, 113−119.

(34) Bar-Cohen, Y.; Bao, X. Q.; Sherrit, S.; Lih, S. S.; Characterization of the Electromechanical Properties of Ionomeric Polymer-Metal Composite (IPMC), Smart Structures and Materials 2002: Electroactive Polymer Actuators and Devices (EAPAD), 2002; Conference Volume *4695*, pp 286−293

(35) Dziewonski, P. M.; Grzeszczuk, M. Impact of the electrochemical porosity and chemical composition on the lithium ion exchange behavior of polypyrroles (ClO_4^-, TOS^-, $TFSI^-$) prepared electrochemically in propylene carbonate. Comparative EQCM, EIS, and CV Studies. *J. Phys. Chem. B* **2010**, *114*, 7158−7171.

(36) Yoshimitsu, Z.; Nakajima, A.; Watanabe, T.; Hashimoto, K. Effects of surface structure on the hydrophobicity and sliding behavior of water droplets. *Langmuir* **2002**, *18*, 5818−5822.